Lateral-torsional buckling resistance prediction model for steel cellular beams generated by Artificial Neural Networks

Felipe Piana Vendramell Ferreira*[a], Rabee Shamass[b], Vireen Limbachiya[b], Konstantinos Daniel Tsavdaridis[c], Carlos Humberto Martins[a]

[a] Department of Civil Engineering, State University of Maringá, Av. Colombo nº 5790, Maringá, Paraná, Brazil

[b] London South Bank University, School of Built Environment and Architecture, London, UK

[c] Department of Civil Engineering, School of Mathematics, Computer Science and Engineering, City, University of London, Northampton Square, EC1V 0HB, London UK

*Corresponding author

E-mail address: fpiana@live.com; fpvferreira2@uem.br (F. P. V. Ferreira), shamassr@lsbu.ac.uk (R. Shamass), limbachv@lsbu.ac.uk (V. Limbachiya), konstantinos.tsavdaridis@city.ac.uk (K. D. Tsavdaridis), chmartins@uem.br (C. H. Martins)

Abstract

The present paper aims to develop an Artificial Neural Network (ANN) formula to predict the LTB resistance of steel cellular beams. A finite element model is developed and validated through experimental tests. A parametric study is then conducted. 768 models are employed to train the ANN. The results are compared with the analytical models, as well as the equation predicted by ANN. The ANN model with seven neurons can accurately predict the LTB resistance of cellular beams as well the LTB combined with web-post buckling or web distortional buckling modes. Hence, the ANN-based formula can be adopted as design tool.

Keywords: Artificial neural network; Machine learning; Steel cellular beams; Lateral-torsional buckling; Finite element method.

Notation

The following symbols are used in this paper:

A_f	the flange area;
A_w	the web area;
b_f	the flange width;
b_w	the web post width;
b_{we}	the width end post;
C_1 and C_2	the coefficients associated to the bending moment diagram and the load at cross-section position
C_b	the modifying factor for the non-uniform bending moment diagram;
C_w	the warping constant;
D_o	the opening diameter
d	the parent section height;
d_g	the cellular beam height;
E	the modulus of elasticity;
G	the shear modulus;
I_z	the moment of inertia about the weak axis;
J	the torsional constant;
k_t	the torsional restraint factor;
k_l	the factor that considers the position of the load;
k_r	the factor that leads to the restriction of rotation
l_e	the effective length ($k_t k_l k_r L$);
L	the length;
M_A, M_B, M_C	the moments located at $L_b/4$, $L_b/2$ and $3L_b/4$, respectively;
M_{pl}	the plastification moment;
p	the length between the opening diameter centers;
t_f	the flange thickness;
t_w	the web thickness;
z_g	the distance from the point of load application to the shear center;
W_y	the plastic modulus about the strong axis;
$W_{el,y}$	the elastic modulus about the strong axis;
$W_{el,z}$	the elastic modulus about the weak axis;
α_{LT}	the imperfection factor;
α_m	the bending moment diagram modifying factor;
α_s	the slenderness reduction factor;
χ_{LT}	the reduction factor;
λ_{LT}	the non-dimensional slenderness, considering LTB resistance;
λ_z	the non-dimensional slenderness about weak axis, considering normal resistance;

1. INTRODUCTION

Steel cellular beams are those with periodical circular web openings. Such beams are manufactured from a parent section in three stages: two thermal cutting lines, separating of the tee sections and welding. The final result is a cross-section with greater bending stiffness than the parent section. Advantages in the use of steel cellular beams in structural design can be highlighted, such as the reduction of the structural system's own weight, the presence of openings favoring the air flow, as well as the passage of ducts for the integration of services which results to the reduction of the structural depth per floor, thus the reduction of the floor to ceiling height.

Authors, such as Ellobody [1], El-Sawy et al. [2] and Ferreira et al. [3], observed that the cellular steel beams are more susceptible to global and local buckling modes, such as the lateral-torsional (LTB), lateral-distortional (LDB) and the web-post (WPB), or even the combination of these failure modes. The LTB occurs in steel cellular beams, which are subject to bending about the strong axis, due to the lack of lateral restraint. The main parameter that favors this type of buckling is the ratio between the unrestrained length of the beam and the radius of gyration about the weak axis (L_b/r). According to studies carried out by Bradford [4–7] the LDB is a phenomenon that takes place for slender web sections, a factor that reduces the torsional stiffness. The hypothesis that the plane section remains plane after deformation, in this case, is not valid. References, such as Kerdal and Nethercot [8], Tsavdaridis and D'Mello [9], Erdal and Saka [10], Panedpojaman et al. [11] and Grilo et al. [12], verified that the WPB, which is characterized by lateral displacement combined with torsion, occurs for steel cellular beams with reduced web-post width and web thickness. Several projects investigated the LTB resistance of cellular steel beams in compared to analytical models, such as EC3 [13], AS 4100-1998 [14], Panedpojaman et al. [15] and Taras and Greiner [16] with Sonck [17].

In the recent years, researchers have utilized artificial intelligence methods such as fuzzy logic, genetic algorithm and artificial neural network (ANN) to solve complex engineering problems. Each method has its advantages; however, it has been stated that ANN is able to provide more accurate predictions [18,19]. ANN is an effective tool that can be used to define nonlinear relations between the inputs and the corresponding outputs and consists of 3 layers. The input layer and output layer are interconnected through the hidden layer, which consists of neurons that are dependent on the set up of the model and each neuron develops a weighted connection between the input and output parameter to define relationships. ANN has been successfully employed to accurately obtain the plastic buckling resistance of steel structures.

More recently, Limbachiya and Shamass [20] predicted the web-post bucking resistance of cellular beams employing ANN. A variation in input parameters and the number of neurons in the hidden layer was reviewed to develop the most accurate model. The experimental and finite element results were used to train the ANN models. It was concluded that ANN provides results that are more in line with test results than those predicted from SCI P355 [21]. Nguyen et al. [22] used ANN to predict the load-bearing capacity of castellated steel beams CSB and they concluded that ANN model with 1 hidden layer and 1 neuron was sufficient to predict the load-carrying capacity of CSB with excellent accuracy in comparison with the experimental results. Hosseinpour et al. [23] developed reliable ANN model that predicted the ultimate moment capacity of castellated beams subjected to lateral-distortional buckling mode. Sharifi et al. [24] tested different ANN training algorithms, and several neurons in the hidden layer to predict the LTB of simply supported cellular steel beams subjected to four-point bending. The authors found that Levenberg–Marquardt training algorithm provided the best performance. Abambres et al. [25] proposed an ANN-based formula that precisely predicted the elastic buckling resistance of simply supported cellular beams subjected to uniformly distributed load. They found that ANN accurately predicted the capacity with maximum and average relative errors of 3.7% and 0.4%, respectively. Sharifi et al. [26] used 99 finite element models to train an ANN model that predict the LTB of cellular beam. In this context, the cellular steel beams were considered to be simply supported and subjected to four-point bending. The predictions of the LTB resistance of steel cellular beams

were compared with the AS 4100-1998 [14]. The results showed that the ANN-based equation proposed by the authors was able to estimate the behavior of cellular steel beams subjected to LTB. Tohidi and Sharifi [27] employed ANN to predict the inelastic lateral-torsional buckling capacity of corroded web opening steel beams. The input and output parameters were defined based on the numerical results from the validated FEM and the data was used for training, validation and testing was 60%, 20% and 20% respectively. The study concluded that even with a small amount of data, ANN was able to predict the target values to an acceptable level of accuracy and provided an assessment method that would provide a fast and reliable decision regarding the future of corrosion damaged I-beam. Gholizadeh et al. [28] developed a back propagation neural network using data from 140 FE models to assess the load carrying capacity of castellated steel beams. Geometric parameters of the beam were used as the input parameters, and when altering the number of neurons within the hidden layer, it was stated that best results were obtained by employing 4 neurons. FE models were also used to develop 140 models that could be used to predict the inelastic distortional buckling capacity assessment of steel I-beams using ANN [29]. 10 models with 6 input parameters, 1 output parameter, 1-10 neurons in the hidden layer were all trained using the Levenberg-Marquardt back propagation algorithm. In a comparison between current design rules (AISC/AISC 360-16 [30], AS 4100-1998 [14] and EC3 [13]), the proposed ANN equation and experimental results, it was concluded that the proposed equation provided more reliable predictions in comparison to the codes. Overall, ANN has many advantages, not only does it provide reliable and accurate results in comparison to the current codes, but it is also providing a simple method which is easier and practical for engineers to use and apply when compared to FE modeling. The data is also crucial, as the statistical accuracy of the model will improve with a greater database and a variability in the input parameters.

As shown so far, there is no application of ANN in post-buckling analysis of steel cellular beams, considering the variation of the type of loading (neutral and destabilizing effect), as well as the combination of LTB with other buckling modes, such as LTB+WPB and LTB+WDB. This paper aims to apply an ANN to predict the LTB resistance of steel cellular beams under combined buckling modes. For this task, a finite element model based on experimental results was developed. A parametric study is carried out considering three steel profiles for the parent section. Geometric parameters such as unrestrained length (L_b), ratio of web-post width to opening diameter (p/D_o), ratio of opening diameter to parent section height (D_o/d), and expansion factor (d_g/d) were varied. Cellular steel beams are usually designed as and herein considered as simply supported and subjected to neutral and destabilizing effects of loading. Three loading conditions were also considered, pure bending, mid-span concentrated load, and uniformly distributed load. From the results, 768 models that had the failure mode governed by LTB, LTB+WDB and LTB+WPB were selected for the development of the ANN model. For the ANN model, the input parameters were defined based on the geometric parameters of the cellular beams, the hidden layer reviewed several neurons within it to define the most accurate and efficient model that could be easily used in real practice while the output parameter was the LTB moment resistance. Finally, the resistance prediction model developed by ANN is compared with finite element models and analytical procedures to assess the accuracy and define the impact of input parameters on the output.

2. BACKGROUND

In this section, the studies, that were developed to investigate the LTB of steel cellular beams, will be presented. In this context, few experimental studies [17,31–33] and many numerical studies based on the finite element method [1,2,35–41,3,15,24,26,31–34] were published.

Regarding experimental studies, Nseir et al. [33] and Boissonnade et al. [32] presented two tests to evaluate the LTB resistance. The cellular beams were simply supported and subjected to four-point bending. The cellular sections were fabricated from HEA340 and IPE330 parent sections, and with total length of 7.5m, and 11m, respectively. Both specimens governed by the LTB, and their peak load was 1977kN and 176.9kN, for HEA340 and IPE330, respectively. Sonck [17] and Sonck and Belis [31] conducted three tests, also considering four-point bending. Three lengths were considered, that of 3.15m, 3.99m and 6.09m. All specimens governed by the LTB, and the maximum peak load was 23.6kN.

Regarding finite element studies, Sweedan [34] performed elastic analyses to investigate the moment-gradient factor, which is a coefficient that takes into account the non-uniform distribution of bending moment along the beam unrestrained length [42]. After evaluating three types of loads on the elastic analyses, a new coefficient that takes into account the bending moment distribution in the unrestrained length was proposed, as well as the geometric parameters of the steel cellular beam. The LTB phenomenon in elastic regime is written according to **Eq. (1)** [43]:

$$M_{cr,0} = \frac{\pi}{L}\sqrt{EI_z GJ + \left(\frac{\pi}{L}\right)^2 EI_z EC_w} \tag{1}$$

Later, El-Sawy et al. [2] presented the inelastic analyses. In this study, the numerical model responses were evaluated as a function of a coefficient, the dimensionless lateral-torsional stiffness, and the LTB combined with WDB and WPB. According to the results, LTB was obtained for k_e<0.5, since the smaller the value of k_e, the greater will be the ratio between the radius of gyration about the weak axis and the unrestrained length. Sonck et al. [35] performed a parametric study to investigate the effects of plastic behavior on steel cellular beams employing finite element method. It was concluded that for short steel cellular beams, the failure mode was governed by the plastic behavior, that was, no buckling phenomenon was observed such as LTB. In Ellobody [1] a parametric analysis were developed to study the behavior of steel cellular beams, considering the combination of buckling modes. In this study, the numerical models results were compared with the AS 4100-1998 [14] specification (**Eqs. 2-5**) and it concluded that such specification underestimated the LTB-resistance of steel cellular beams.

$$M_{Rk} = \alpha_m \alpha_s M_{pl} \le M_{pl} \tag{2}$$

$$\alpha_m = \frac{\sqrt{3}M_{máx}}{\sqrt{\left[\left(M_A\right)^2 + \left(M_B\right)^2 + \left(M_C\right)^2\right]}} \le 2.5 \tag{3}$$

$$\alpha_s = 0.6\left\{\sqrt{\left[\left(\frac{M_{pl}}{M_o}\right)^2 + 3\right]} - \left(\frac{M_{pl}}{M_o}\right)\right\} \quad (4)$$

$$M_o = \sqrt{\left\{\left(\frac{\pi^2 EIy}{l_e^{\,2}}\right)\left[GJ + \left(\frac{\pi^2 EC_w}{l_e^{\,2}}\right)\right]\right\}} \quad (5)$$

Boissonnade et al. [32] carried out a parametric study to investigate the design recommendations to LTB provided by ArcelorMittal ACB+ [44]. Such procedure underestimates the resistance of steel cellular beams under LTB, since it only considers the stiffness of the upper tee. In this context, the authors recommended the EC3 [45] procedure (**Eqs. 6-10**), using the buckling curve *c* to calculate the LTB resistance.

$$M_{Rd} = \frac{\chi_{LT} W_y f_y}{\gamma_{M1}} \quad (6)$$

$$\chi_{LT} = \frac{1}{\phi_{LT} + \sqrt{\phi_{LT}^{\,2} - \lambda_{LT}^{\,2}}} \leq 1.0 \quad (7)$$

$$\phi_{LT} = 0.5\left[1 + \alpha_{LT}\left(\lambda_{LT} - 0.2\right) + \lambda_{LT}^{\,2}\right] \quad (8)$$

$$\lambda_{LT} = \sqrt{\frac{W_y f_y}{M_{cr}}} \quad (9)$$

$$M_{cr} = C_b M_{cr,0} \quad (10)$$

In Sonck and Belis [31], the effect of residual stresses on LTB resistance was investigated. The authors observed that calculation recommendations that do not consider such effect on the structural behavior of steel cellular beam under LTB may be unsafe. In this scenario, Sonck [17] based on EC3 [45] proposed a new imperfection factor for the calculation of resistance to LTB. The use of α_{LT}=0.6 was proposed based on EC3 [45], and according to the formulations of Taras and Greiner [16], two coefficients were proposed, considering the relations d_g/b_f>1.2 (**Eq. 11**) and d_g/b_f≤ (**Eq. 12**).

$$\alpha_{LT} = 0.18\sqrt{\frac{W_{el,y}}{W_{el,y}}} \leq 0.64 \quad (11)$$

$$\alpha_{LT} = 0.25\sqrt{\frac{W_{el,y}}{W_{el,y}}} \leq 0.64 \quad (12)$$

In Panedpojaman et al. [15] inelastic analyses were developed to investigate the LTB resistance of steel cellular beams. The authors highlighted the influence of shear stresses for short spans, models for which the resistance can be characterized as WPB or some plastic mechanism. In this context, the authors proposed a correction coefficient to calculate the LTB resistance, according

to the methodology described in EC3 [45], using the buckling curve *b*. **Eqs. (8-9)** present the calculations of the coefficients, considering the absence and presence of shear loads, respectively.

$$M_{Rd} = k_{LB} \frac{\chi_{LT} W_y f_y}{\gamma_{M1}} \tag{13}$$

$$k_{LB} = \frac{1}{-0.01\lambda_{LT} + 1.05} \tag{14}$$

$$k_{LB} = \frac{min\left[\left(0.16\frac{A_f}{A_w} + 0.66\right),(1.0)\right]}{max\left[\left(-0.1\lambda_{LT} + 1.13\right),(0.9)\right]} \tag{15}$$

Ferreira et al. [3] developed a parametric study to investigate the LTB resistance, considering the effect of loading applied at the upper flange (destabilizing effect) as well as at the shear centre (neutral effect). The results of this study were compared with calculation models existing in the literature [14–16,31,45]. The work highlighted that the combination of the Taras and Greiner [16] model with the Sonck factor [17] is a good approximation for the LTB resistance of steel cellular beams. The equations combined between Taras and Greiner [16] with the Sonck factor [17], considering loads applied at shear centre are described below (**Eqs. 16-18**). For loads applied at the upper flange, the equation of the three factors (C_1, C_2 and C_3) is used to calculate the critical moment [46] (**Eq. 19**).

$$\phi_{LT} = 0.5\left[1 + \left(\frac{\lambda_{LT}^{\ 2}}{\lambda_z^{\ 2}}\right)\alpha_{LT}\left(\lambda_z - 0.2\right) + \lambda_{LT}^{\ 2}\right] \tag{16}$$

$$\lambda_{LT} = \sqrt{\frac{W_y f_y}{M_{cr}}} \tag{17}$$

$$\lambda_z = \sqrt{\frac{Af_y}{N_{cr}}} \tag{18}$$

$$M_{cr} = C_1 \frac{\pi^2 EI_z}{L^2}\left[\sqrt{\frac{C_w}{I_z} + \frac{L^2 GJ}{\pi^2 EI_z} + \left(C_2 z_g\right)^2} - C_2 z_g\right] \tag{19}$$

Later, Ferreira et al. [37] investigated the Load and Resistance Factor Design (LRFD), which is based on the ANSI/AISC 360-16 [30] design procedure, for steel cellular beams under LTB. The authors observed that for intermediate spans, the American standard overestimates the LTB resistance, since the LRFD value is equal to 0.9. In this context, the average LRFD value calculated by the authors was 0.83. Komal et al. [36] presented an extensive parametric study of steel cellular beams in which buckling and post-buckling analyses were performed. The authors showed that the unrestrained length is an important parameter, since the lateral displacement is directly influenced by the compressed flange, thus causing LTB. Khatri et al. [39] investigated the effect of the load

position on the cross-section by carrying out elastic analyses, considering the effect of stabilizing, neutral and destabilizing on the moment-gradient factor. In this study, the authors observed the moment-gradient factor variation as a function of the buckling modes that were governed by the combination of LTB+WDB and for short spans. Bhat and Gupta [40] carried out a parametric study, considering simply supported cellular beams subjected to four-point bending. The results of this study were compared with the recommendation of the Indian standard IS 800:2007 [47], that is applied to common steel beams. The authors showed that the Indian standard was conservative for cellular steel beams with a yield strength of 250 MPa. However, for cellular steel beams with yield strengths of 350MPa and 450MPa, this comparison was unconservative. Recently, Faria et al. [41] investigated the LTB resistance in fire situations by performing finite element analyses. The authors presented a procedure to predict the LTB resistance of cellular steel beams, considering fire and room ambient temperature (**Eq. 20**) situations. Such calculation methodology is a modification of the equations presented in EC3 [45].

$$\phi_{LT} = 0.5\left[1+0.25\left(\lambda_{LT}-0.2\right)+\lambda_{LT}^{\ 1.9}\right] \tag{20}$$

As presented so far, few researchers have conducted experimental studies, whereas most of them presented numerical studies and sought alternatives to calculate the LTB resistance of steel cellular beams. In this case, revisions were made to LTB-resistance calculations for steel beams without web openings. It is important to highlight that the procedures for calculating the LTB resistance of steel profiles without web openings are very well consolidated. As an example, studies that made EC3 [45] revisions were highlighted, in order to accurately present the numerical response with the calculation procedures. Finally, although many alternatives were presented to calculate the LTB resistance of steel cellular beams, it is a complex procedure, since these perforated beams can fail due to the interaction of buckling modes. Consequently, the present study employs the power of artificial neural network algorithms, seeking the calculation of LTB resistance while considering the interaction between the buckling modes.

3. FINITE ELEMENT MODEL: VALIDATION AND PARAMETRIC STUDIES

In this section, the validation results will be briefly presented, as well as the geometric parameters that were considered in the parametric study. This is because the paper focuses on the artificial neural network.

For the validation study, eight experimental models of steel cellular beams [9,31,32,48,49] were considered. All steel cellular beams are simply supported. Elastic-perfectly plastic material behavior was considered in the numerical models, and the cellular beams were modeled with 10mm S4R shell elements, according to the ABAQUS® software library [50]. The models were processed in two stages: buckling and post-buckling analyses. Many researchers have used this procedure to analyze buckling problems in steel cellular beams [36,51]. The buckling analysis predict the critical buckling load and its respective buckling mode. It is noteworthy that no initial imperfections are considered here. Subsequently, the buckling mode response from the analysis performed in the first stage is used as an initial geometric imperfection for the subsequent post-buckling analysis ($d_g/100$ if $L/d_g<10$ and $L/1000$ if $L/d_g\geq10$) [3]. Residual stresses were considered [52]. The imperfections are inserted with the commands

*IMPERFECTION and *INITIAL CONDITIONS, TYPE=STRESS for initial geometric imperfection and residual stresses, respectively. The post-buckling analysis is performed by *Static Riks*, which uses the arc length method.

Regarding the validation results, the numerical results obtained showed the same failure mode as the experimental models. In **Fig. 1**, key examples of the failure modes are presented. Beam 2 test also performed by Surtees and Liu [48] failed by WDB+WPB. These modes were verified in the final configuration of the numerical model, as shown in **Fig. 1a**. 4B test, which was carried out by Warren [49], governed by WPB. This mode was observed in the finite element model presented in **Fig. 1b**. Tests A1 and B1, which were conducted by Tsavdaridis and D'Mello [9], failed by WPB. **Fig.1c**, in the same way, depict the failure modes of the developed finite element models. Boissonnade et al. [32] and Sonck and Belis [31] performed LTB tests; **Fig. 1d**, **Fig. 1e** and **Fig. 1f** depict the final mode shape of these finite element models for IPE 330, CS2_L3 and CS2_L4, respectively. It is concluded that the finite element models developed for the validation study were in agreement with the failure modes of the tests. Also, the force against mid-span vertical displacement relationships were made to compare with the tests (**Fig 2**), and the results are summarized in **Table 1**.

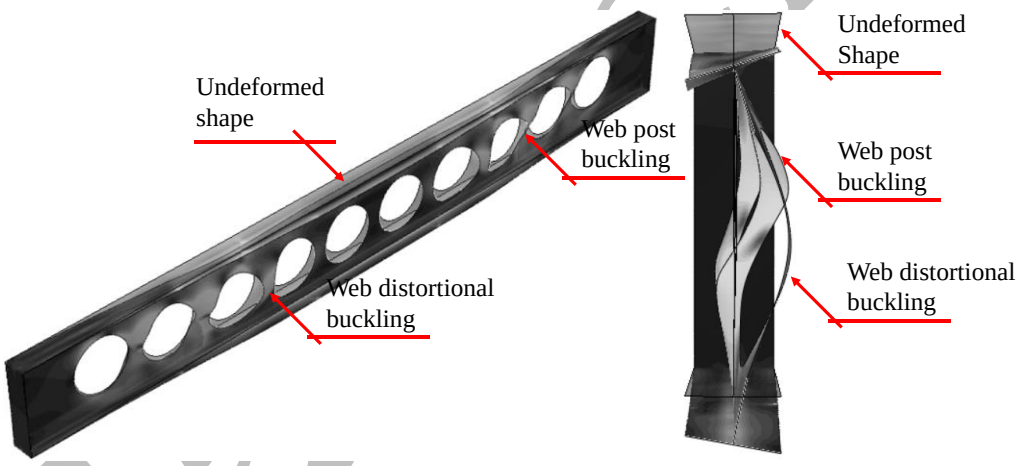

(a) Beam 2

(b) 4B

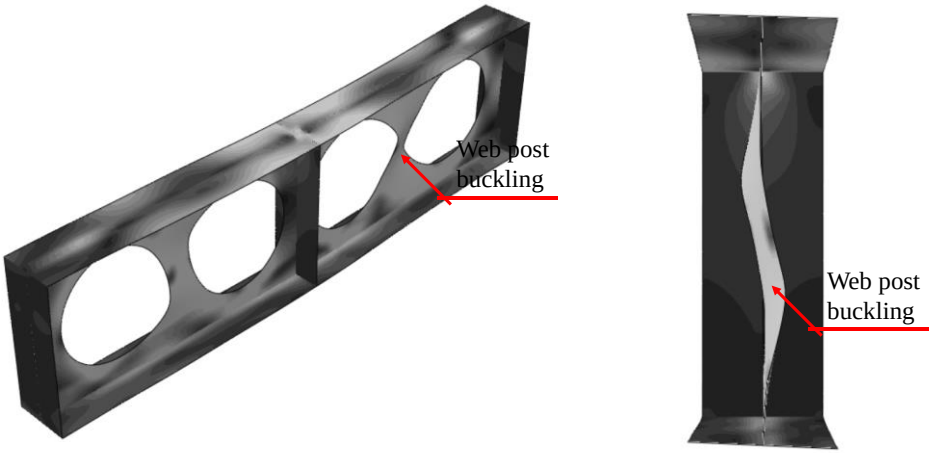

(c) A1

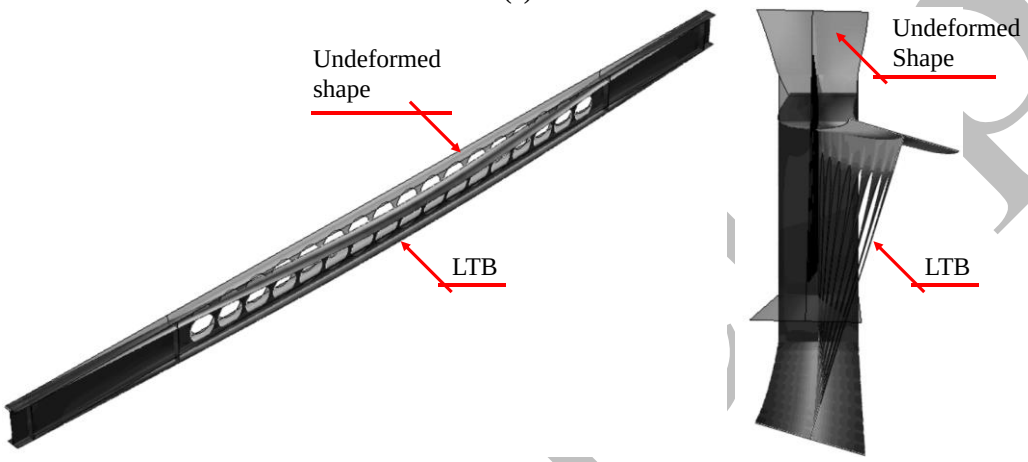

(d) IPE 330

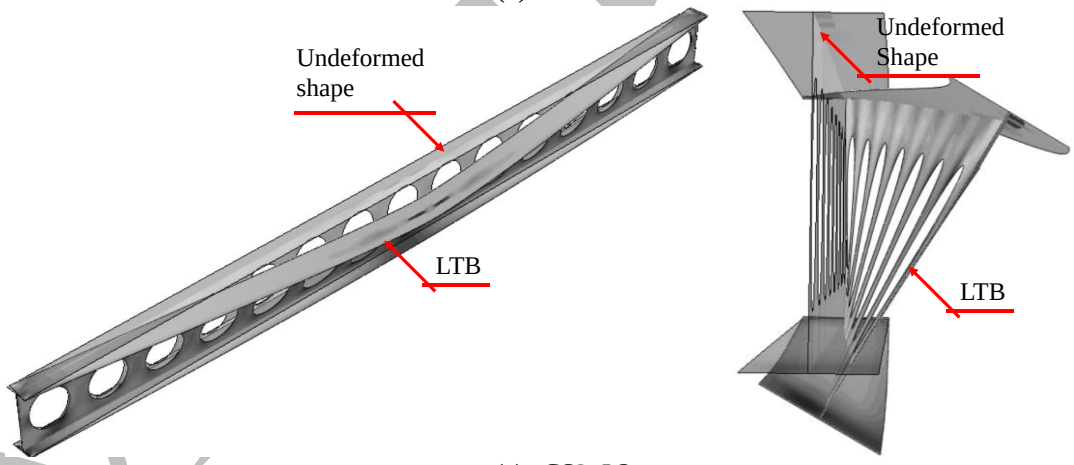

(e) CS2_L3

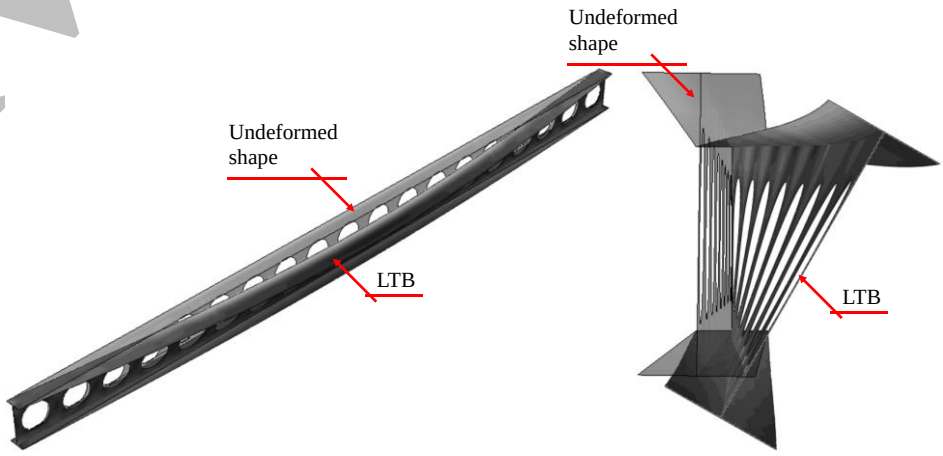

(f) CS2_L4

Fig. 1: Final configuration of finite element models

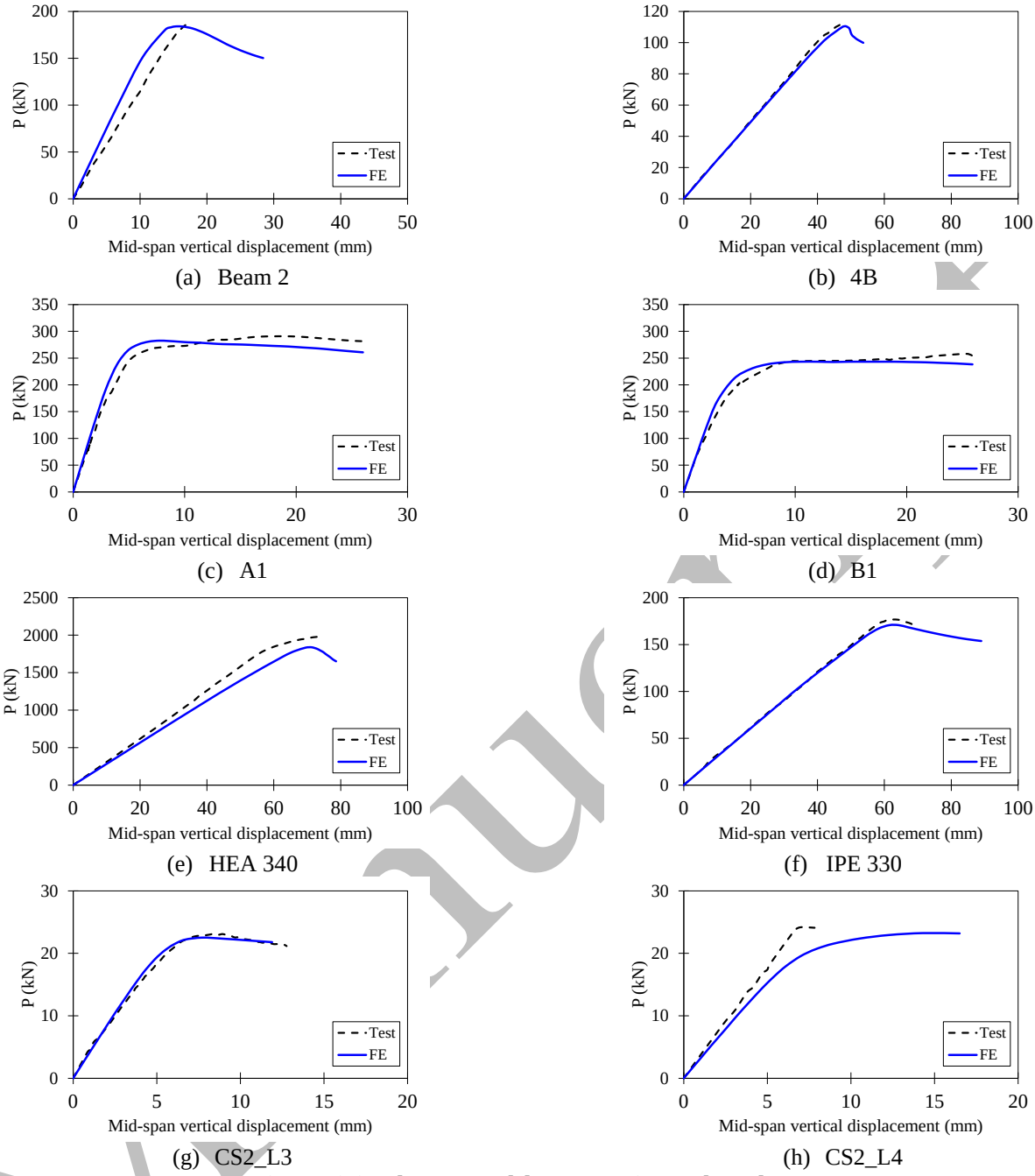

Fig. 2: Finite element models vs. experimental results

Table 1: Validation results

Test	Reference	Test		Finite element model		$1-P_{Test}/P_{FE}$ (%)
		P_{Test} (kN)	Failure mode	P_{FE} (kN)	Failure mode	
Beam 2	Surtees and Liu [48]	188.5	WDB+WPB	184.0	WDB+WPB	-2.4
4B	Warren [49]	114.0	WPB	110.5	WPB	-3.2
A1	Tsavdaridis and D'Mello [9]	288.7	WPB	282.5	WPB	-2.2
B1	Tsavdaridis and D'Mello [9]	255.0	WPB	243.1	WPB	-4.9
HEA 340	Boissonnade et al. [32]	1,977.0	LTB	1,838.4	LTB	-7.5
IPE 330	Boissonnade et al. [32]	176.9	LTB	170.7	LTB	-3.6
CS2_L3	Sonck and Belis [31]	22.3	LTB	22.5	LTB	0.9
CS2_L4	Sonck and Belis [31]	23.6	LTB	23.2	LTB	-1.7

In the parametric study, the ASTM A572 Grade 50 steel is considered. **Fig. 3** presents the geometrical parameters that were varied (**Table 2**). Cellular beams are considered as simply supported and subjected to three types of loadings applied to the shear centre (i.e., uniform bending, mid-span concentrated load and uniformly distributed loads) considering the neutral effect, and two types of loading applied to the upper flange (i.e., mid-span concentrated load and uniformly distributed loads) to simulate the destabilizing effect.

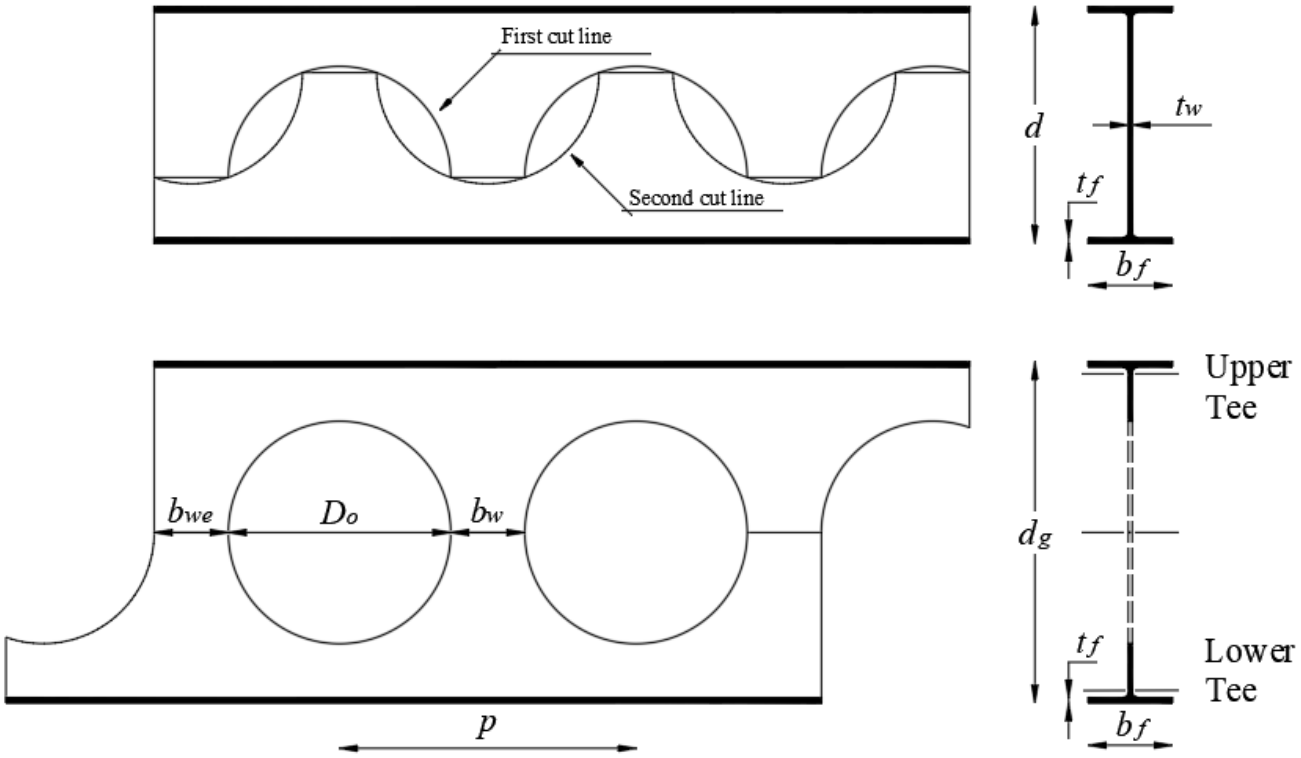

Fig. 3: Geometrical parameters, adapted from [53]

Table 2: Parameters

Parameter	Variation
p/D_o	1.2 and 1.45
D_o/d	0.95 and 1.15
d_g/d	1.3, 1.35, 1.4, 1.45 and 1.5
Steel sections	W200x22.5, W310x32.7 and W530x85
Loading type	Neutral effect: uniform bending, mid-span concentrated load and uniformly distributed loads Destabilizing effect: mid-span concentrated load and uniformly distributed loads

The parametric study in 768 models allowed to identify the failure mode governed either by LTB (**Fig. 4a**) or the combination of this failure mode with other buckling modes, such as LTB+WDB (**Fig. 4b**) and LTB+WPB (**Fig. 4c**). The results of the 768 models are used for the development of a robust ANN formula as described below.

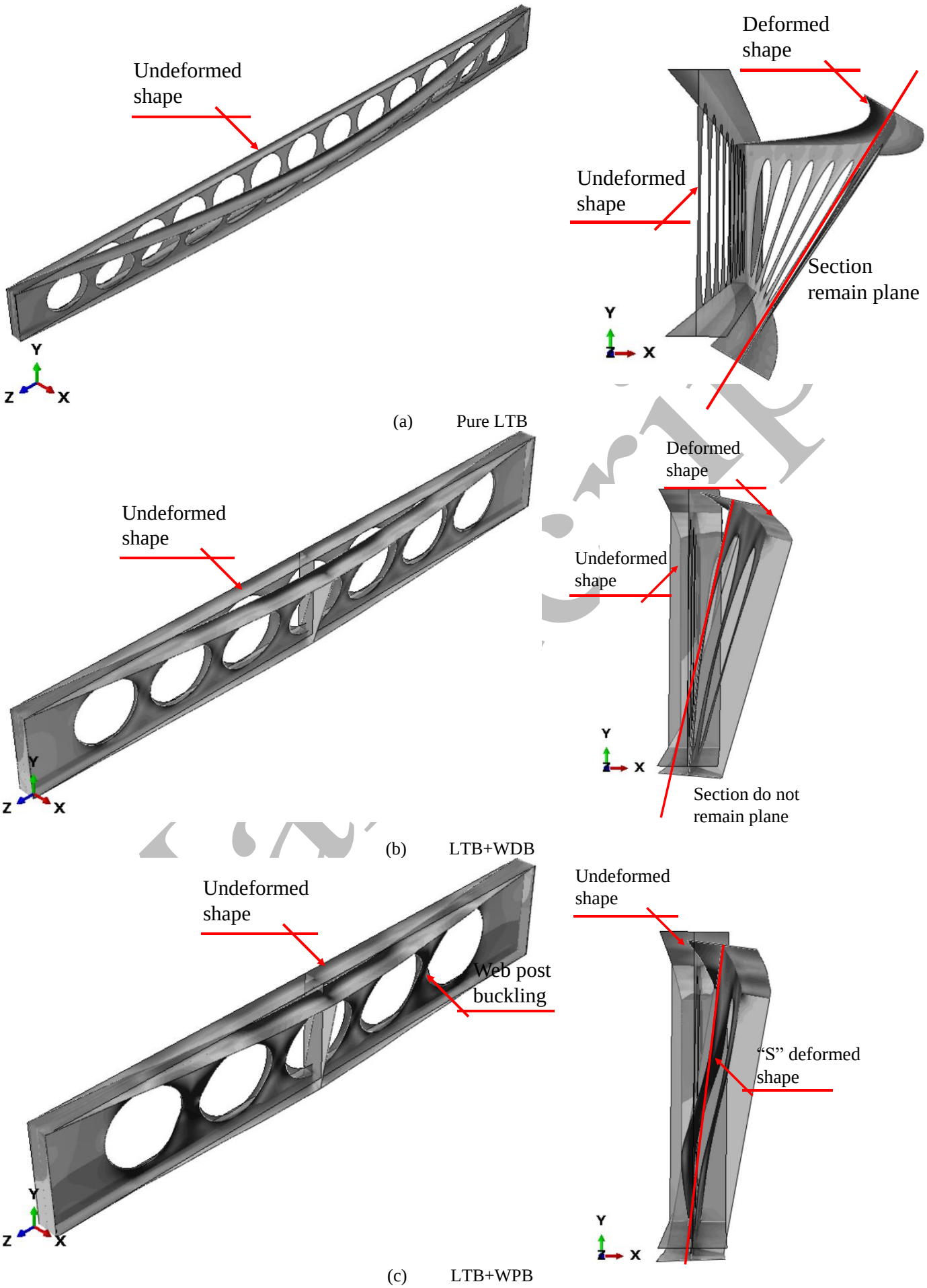

Fig. 4: Failure modes

4. DEVELOPMENT OF THE ARTIFICIAL NEURAL NETWORK (ANN)

In this section, the development of the artificial neural network is presented.

4.1 NEURAL NETWORK ARCHITECTURE

The general architecture of an ANN includes the input layer, hidden layer, and output layer. The normalized input values are connected to the hidden layer, which consists of neurons that are dependent on the analysis that is conducted. The connection between each input and neuron in the hidden layer is weighted and also consists of constant bias value. The hidden layer is thereafter connected to the output layer. Again, each connection from the hidden layer to the output layer is weighted with a value, a transfer function and a constant bias value. As input values are normalized, the output value will also be normalized and will require denormalization to obtain predicted values that can be compared to the target values. To then assess the accuracy of the model, the errors between the predicted and target values are calculated.

The errors should be minimized by adjusting the weights and bias values of the ANN. This can be achieved by transferring the information (errors) from the output layer towards the input layer of the ANN [54]. This process is called Back-Propagation of Multilayer Feed Forward ANN. In addition, the final weights and bias values between the different layers can be used to quantify the impact of input parameters on the output parameter. The network architecture used in this paper is a Multi-Layer Perceptron Network (MLPN). The neural network toolbox within MATLAB [55] solves a data fitting problem with a two-layer feedforward neural network and is the method that has been adopted in this study.

To derive the ANN model, a number of parameters need to be introduced, herein noted as input parameters as well as the number of neurons within the hidden layer, the activation function, and the output parameter. The input parameters in this study represent the variable geometric characteristics of cellular beam, including the length (L), overall height of the beam (d_g), opening diameter (D_o), distance between opening (b_w), flange width (b_f), flange thickness (t_f), web thickness (t_w), distance from the point of the load application to the shear centre of the section (z_g), and the moment-gradient factor (C_b). In this study, the C_b is taken as presented in DD ENV 1993-1-1 (2002) [46]. For uniformly distributed loading, C_b is equal to 1.132. Considering mid-span concentrated load, C_b is equal to 1.365 while beams with uniform bending the value C_b is equal to 1.0. The output parameter to be predicted is the LTB moment resistance (M).

The number of neurons in the hidden layer has influence on the accuracy of the ANN model. The optimal number of neurons in the hidden layer can be defined by modelling several networks with a different number of the neurons and comparing the differences in the results. In this paper, the ANN network was modelled with 3, 5, 7, 9 and 11 neurons in the hidden layer. **Fig. 5** illustrates an example of an ANN structure consisting of 9 input parameters, 3 neurons in the hidden layer, and 1 output parameter.

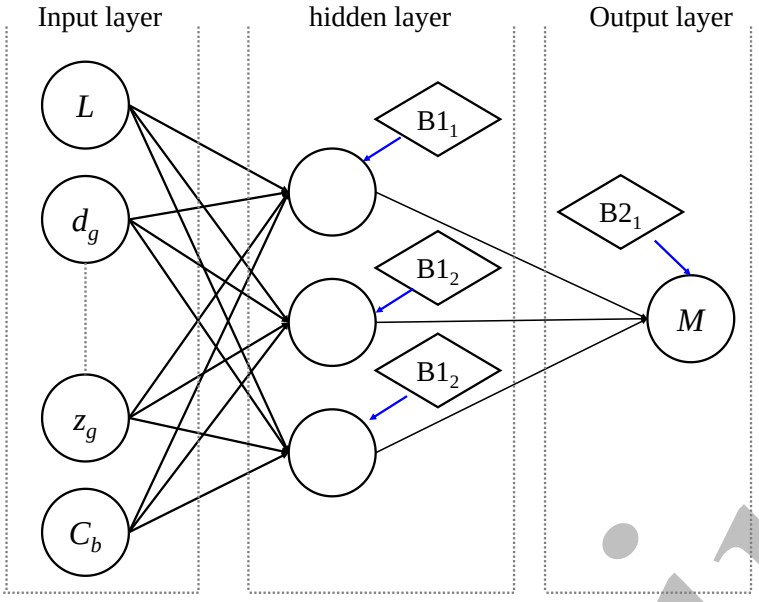

Fig. 5: ANN Model with 3 neurons in the hidden layer

4.2 INPUT AND OUTPUT NORMALIZATION

The progress of training can be reduced if training data define a region that is relatively narrow in some dimensions and elongated in others [25]. Therefore, normalization for variables across all data patterns should be implemented to improve the learning speed, performance, accuracy, and stability of the training process. Both input and target parameters can be normalized using **Eq. (21)** [56], where Y^{act} is the actual value of the input/output, X^{norm} is the value, $X_{\min}$ and $X_{\max}$ are the minimum and maximum values of the input/output parameters, respectively (**Table 3**). $Y_{\min}$ is the minimum value for each row of X (default is –1) and $Y_{\max}$ is the maximum value for each row of X (default is +1).

$$X^{norm} = \frac{\left(Y_{\max} - Y_{\min}\right)\left(X^{act} - X_{\min}\right)}{\left(X_{\max} - X_{\min}\right)} + Y_{\min} \tag{21}$$

Table 3: Parameters used to normalize input and target values

Input/Target Parameter	X_{min}	X_{max}	Y_{min}	Y_{max}
L (mm)	1500	15000	-1	1
d_g (mm)	268	803	-1	1
D_o (mm)	196	616	-1	1
b_w (mm)	47.6	228.6	-1	1
b_f (mm)	102	166	-1	1
t_f (mm)	8	16.5	-1	1
t_w (mm)	6.2	10.3	-1	1
z_g (mm)	0	401.5	-1	1
C_b	1	1.365	-1	1
***M* (kN.m)**	16.71	470.34	-1	1

4.3 LEARNING (TRAINING) ALGORITHM AND TRANSFER FUNCTION

The total number of data sets used in the ANN model was 768. To avoid overfitting the ANN model, the data points are randomly divided into training set, validation set and testing set, with 70%,15% and 15% of the data, respectively. While the training set is used to compute the gradient and update the weights and biases, a process of cross validation takes place using the validation data set so the performance of the network can be generalized. When the optimum network parameters are defined, the test data set is used to assess the ANN accuracy. The Levenberg-Marquardt back propagation training algorithm is adopted in this study as this algorithm is fast, has stable convergence and is suitable for training small- and medium-sized problems. **Eqs. (22-23)** show the hyperbolic tangent transfer function that is required to determine the normalized output value based on the inputs provided [57].

$$O_s = B1_s + \sum_{k=1}^{r}\left(w_{k,l}^{ho} \frac{2}{1+e^{-2H_k}} - 1 \right) \tag{22}$$

$$H_k = B2_k + \sum_{j=1}^{q} w_{j,k}^{ih} \cdot I_j \tag{23}$$

Where, O_s represents the normalized output value, q is the number of input parameters; r is the number of hidden neurons; s is the number of output parameters; $B1_s$ and $B2_k$ are the biases of s^{th} output neuron and k^{th} hidden neuron (H_k), respectively; $w_{j,k}^{ih}$ is the weights of the connection between I_j and H_k; $w_{k,l}^{oh}$ are the weights of the connection between H_k and O_s.

4.4 ASSESSING THE ACCURACY OF NEURAL NETWORK

To assess the accuracy of the output the Regression values (R2), Root Mean Square Error (RMSE) and Mean Absolute Error (MAE) are calculated using **Eq. (24)**, **Eq. (25)** and **Eq. (26**) respectively, where t_i and O_i are the actual and predicted LTB moment resistance of steel cellular beam, and N is the total number of data points in each set of data. $\bar{O}_i$ and $\bar{t}_i$ are the average of the predicted and actual LTB moment resistance.

$$R = \frac{\sum_{i=1}^{N}\left(O_i - \bar{O}_i\right)\left(t_i - \bar{t}_i\right)}{\sqrt{\sum_{i=1}^{N}\left(O_i - \bar{O}_i\right)^2 \sum_{i=1}^{N}\left(t_i - \bar{t}_i\right)^2}} \tag{24}$$

$$RMSE = \sqrt{\frac{\sum_{i=1}^{N}\left(O_i - t_i\right)^2}{N}} \tag{25}$$

$$MAE = \frac{1}{N}\sum_{i=1}^{N}\left|O_i - t_i\right| \tag{26}$$

4.5 QUANTIFYING INPUT VARIABLE CONTRIBUTIONS IN ANN

In this section, the methodology for evaluating the contribution of each variable to LTB resistance of steel cellular beams is presented.

4.5.1 Connection Weight Approach

Olden and Jackson [58] proposed the connection weigh approach that estimates the rank importance of each individual input in the neural network. The magnitude and sign of the weights between neurons identify the effect of the input parameters on the output. The advantage with this approach is that it not only provides the impact of each input parameter, but it also shows whether an increase in the input parameter will increase or decrease the value of the output parameter. A positive value will dictate that an increase in the input parameter will increase the value of the output parameter and vice versa for a negative value. The impact of an input (S_x) can be calculated by the product of raw input-hidden and hidden-output connection weights and sum the products across all hidden neuron [58] as illustrated in the following **Eq. (27)** [59]:

$$Input_X = \sum_{Y=A}^{E} Hidden_{XY} \tag{27}$$

4.5.2 Garson's Algorithm

Garson [60] proposed a method to determine the relative importance of each input variable in the network. This approach has been used in previous studies [57,61–63]. It is important to note that Garson's algorithm uses the absolute values of the connection weights when calculating variable contributions, and hence does not provide the direction of the relationship between the input and output variables [58]. The relative importance of the j^{th} input parameter on the output is presented in **Eq. (28)**, in which *Ni* and *Nh* are the numbers of neurons in the input and hidden layers, respectively; *w* is connection weights; the subscripts *k*, *m*, and *n* refer to input, hidden, and output neurons, respectively, and the superscripts *i*, *h*, and *o* refer to input, hidden, and output layers, respectively.

$$I_j = \frac{\sum_{m=1}^{m=Nh}\left(\frac{w_{jm}^{ih}}{\sum_{k=1}^{Ni} w_{km}^{ih}} w_{mn}^{ho}\right)}{\sum_{k=1}^{k=Ni}\left[\sum_{m=1}^{m=Nh}\left(\frac{w_{km}^{ih}}{\sum_{k=1}^{Ni} w_{km}^{ih}} w_{mn}^{ho}\right)\right]} \quad (28)$$

5. RESULTS AND DISCUSSION

As stated previously, the number of neurons in the hidden layer will have an influence on the ANN accuracy. Although utilizing many neurons in the hidden layers increases the accuracy of the ANN prediction, the model gives more complicated explicit formulas which in practical application create more space for error. Additionally, an increase in the number of neurons may lead to overtraining [61]. **Table 4** provides the R2 and MSE values of the training, validation and testing data that was determined for the different models. As the number of neurons increase there is a direct correlation with the accuracy of the model. However, it can be seen that the model with a low number of neurons still has an exceptionally high level of accuracy. As the models with fewer neurons provide this level of accuracy and will result in a more user-friendly formula for industrial application, it is acceptable that these can be used instead of those models with a higher level of neurons.

Table 4: Comparison of statistical values to evaluate the accuracy of the ANN models with different neurons

Number of neurons	R^2			*MSE*			All data		
	Training	Validation	Testing	Training	Validation	Testing	RMSE	MAE	R^2
3	0.99974	0.99966	0.99973	$8.71\text{x}10^{-5}$	$9\text{x}10^{-5}$	$1.41\text{x}10^{-4}$	2.220	1.510	0.9994
5	0.99985	0.99985	0.99967	$5.01\text{x}10^{-5}$	$7.11\text{x}10^{-5}$	$1.14\text{x}10^{-4}$	2.037	1.382	0.9996
7	0.99987	0.99990	0.99842	$4.17\text{x}10^{-5}$	$3.67\text{x}10^{-5}$	$6.14\text{x}10^{-5}$	1.678	1.075	0.9997
9	0.99990	0.99987	0.99989	$2.79\text{x}10^{-5}$	$3.31\text{x}10^{-5}$	$3.37\text{x}10^{-5}$	1.232	0.839	0.9998
11	0.999996	0.99883	0.99992	$1.25\text{x}10^{-5}$	$4.39\text{x}10^{-5}$	$3.51\text{x}10^{-5}$	1.030	0.604	0.9999

After reviewing the statistical data of the ANN model, the accuracy of the model was assessed based on the overall predicted values of the ANN model and the actual values. The statistical parameters R2, RMSE and MAE of the network with different neuron can be seen in **Table 4**. **Fig. 6a** and **Fig. 6b** are examples of the actual against predicted lateral torsional buckling moment for ANN models with 7 and 9 neurons, respectively. As expected, that as the number of neurons increase the RMSE and MAE reduced and there is a slight change in the regression value. For instance, as the number of neurons increase from 7 to 9 the RMSE decreases from 1.678 to 1.232 and MAE decrease from 1.075 to 0.839 while the regression value slightly improved. Based on these results it

was concluded that an ANN network model with 7 neurons provides a high level of accuracy, as well as a more practical equation and this ANN model will be used for further analysis in the following sections.

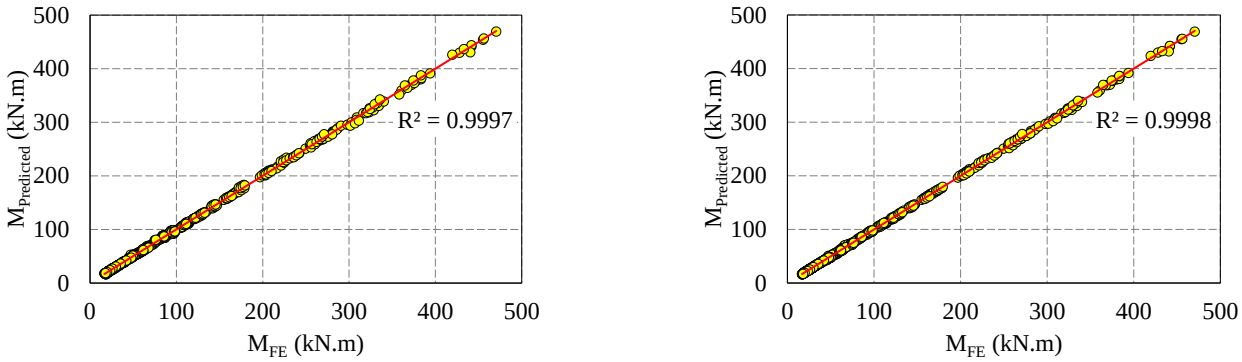

(a) 7 Neurons (b) 9 Neurons

Fig. 6: Actual vs. predicted bending moment

In order to further validate the ANN predictions, the impact of input parameters was assessed using the connection weight approach and Garsons algorithm. **Fig. 7** provides the impact that each input parameter within the ANN model has on the lateral torsional moment capacity of a cellular beam. The connection weight approach shows that input parameters d_g, b_w, b_f, t_f, t_w and C_b have direct impact on the strength – increasing in these parameters results in an increase in bending moment capacity. This agrees with what would have been expected as the greater the height, web-thickness, flange thickness and width and spacing between openings of cellular beam, the greater the lateral torsional buckling resistance. On the other hand, input parameters L, D_o and z_g have negative impact on the resistance as it was anticipated, as increasing the length, and opening diameter, and leads to a decrease in strength and the destabilizing effect reduces the buckling resistance. **Fig. 7** also illustrates the relative importance (S values) of the nine input parameters. The most important input corresponds to highest absolute S value. It can be observed that the length, flange width and web thickness of the cellular beams are the significant factors with detrimental effect on the resistance, while the spacing between opening and opening diameter have less effect on the resistance. It is worth noting that these results do not correlate to the accuracy of the ANN predictions, and it is providing another form of validation for the ANN model. **Fig. 8** shows the contribution (%) of each input parameter (L, d_g, D_o, b_w, b_f, t_f, t_w, z_g, C_b) to output parameter M calculated using Garson algorithm as explained in section 4.5.2. The contribution of these input parameters is 25.22%, 9.79%, 9.62%, 6.48%, 9.40%, 6.85%, 14.26%, 9.43% and 8.94%, respectively, indicting, again, that the length, and web thickness have significant contribution to the resistance. In conclusion, as the ANN model with seven neurons provides predictions with high level of accuracy and the impact of the inputs on the resistance is as physically expected, it will be used in the following sections.

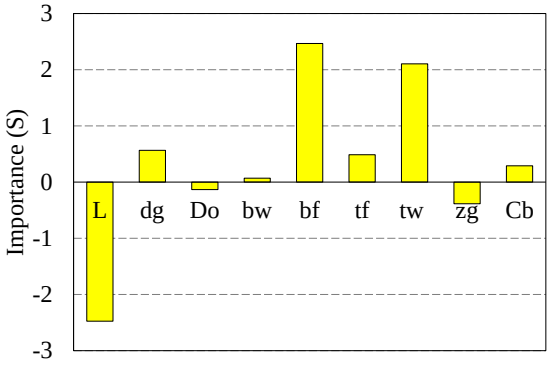

Fig. 7: Impact of input parameters on the resistance

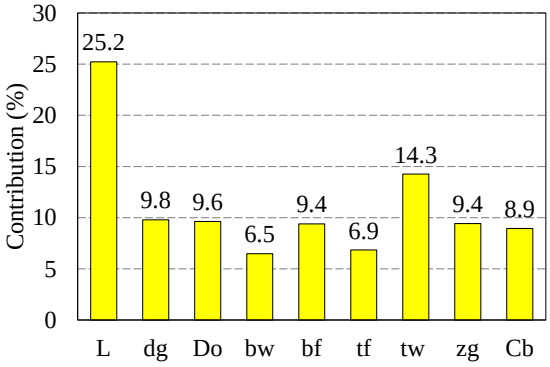

Fig. 8: Contribution (%) of input parameters to the resistance

6. ANN-BASED FORMULA AND COMPARATIVE ANALYSES

In this section the resistance prediction results developed by ANN are compared with analytical procedures. ANN-based formula to predict the normalized LTB moment resistance is illustrated in the **Eq. (29)**. The input parameters, which would have to fall within X_{max} and X_{min} range stated in Table 3, should be normalized using **Eq. (21)**. In order to calculate the normalized LTB moment resistance $(M)_n$, the values H_1, H_2…H_7 should be calculated using **Eq. (30)** and substituted into **Eq. (29)**. In the equations, $(M)_n$ represent the normalised value of the input parameter, *w1(i,j)* are the connection weights between neuron in the hidden layer (i) and input (j), as seen in the **Table 5**, *w2(i)* are the connection weights between the neuron in the hidden layer (i) and the output, as seen in the **Table 5**. *B1(i)* are the bias for each neuron (i) in the hidden layer, as seen in the **Table 5**, B2 is the output bias and is equal to 1.96889. To determine the LTB moment resistance to its original format (i.e., without normalisation), denormalization need to be conducted.

$$\left(M\right)_n = B2 + \sum_{i=1}^{n=7} w2(i)\left(\frac{2}{1+e^{-2Hi}} - 1\right) \tag{29}$$

$$H_i = B1(i) + W1(i,1)(L)_n + w1(i,2)(d_g)_n + w1\left(i,3\right)\left(D_o\right)_n + w1\left(i,4\right)\left(b_w\right)_n + w1\left(i,5\right)\left(b_f\right)_n + w1\left(i,6\right)\left(t_f\right)_n + w1\left(i,7\right)\left(t_w\right)_n + w1\left(i,8\right)\left(z_g\right)_n + w1\left(i,9\right)\left(C_b\right)_n \tag{30}$$

Table 5: The connection weight and the bias values

Neuron	*w1(i,j)*									*w2(i)*	*B1(i)*
	L	d_g	D_o	b_w	b_f	t_f	t_w	z_g	C_b	***M***	
1	-0.2669	0.1919	0.0195	-0.0464	-0.3124	-0.6813	0.9791	1.5399	-0.9908	-0.0504	1.4748
2	-1.7443	0.2162	-0.6503	-0.3029	-0.7204	-0.1041	-1.2666	-0.1281	-0.3717	-2.1171	-3.2841
3	0.6228	-0.7600	-0.5885	-0.3327	0.1577	-0.1627	-0.6824	-0.0555	0.1633	-0.1882	-1.1741
4	-1.0510	0.7635	-0.4885	1.2044	0.0841	-0.1215	0.7132	-1.2802	-1.0535	-0.0020	1.3307
5	0.8900	-0.2046	0.0635	0.0006	0.1224	-0.3040	-0.2837	0.1261	-0.1031	-2.8734	1.8707
6	-1.5960	0.2017	-0.6648	-0.3083	0.3822	-0.3031	-0.6035	-0.1166	-0.3515	2.4490	-1.6562
7	1.2305	-0.5902	0.5826	0.2080	1.1378	0.2109	0.0242	0.1690	0.1394	0.3250	1.5917

6.1. LOADS APPLIED AT SHEAR CENTRE

The equation developed by ANN is compared with the EC3 [13], AS 4100-1998 [14], Panedpojaman et al. [15], EC3 [13] and Sonck [17], Taras and Greiner [16] with Sonck [17] and Faria et al. [41] procedures, considering loads applied at shear center. It is important to highlight that of the 768 models that were selected for the application of the ANN, 458 models were subjected to loading applied at shear centre. The comparation results are presented in **Fig. 9.**

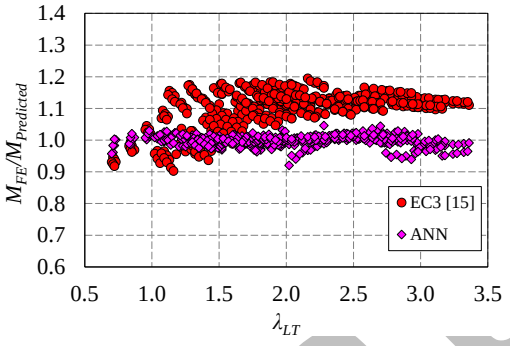

(a) ANN vs. EC3 [13]

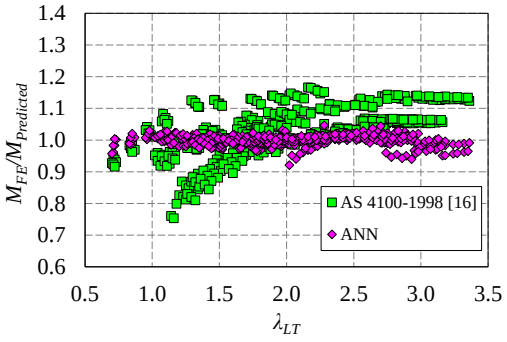

(b) ANN vs. AS 4100-1998 [14]

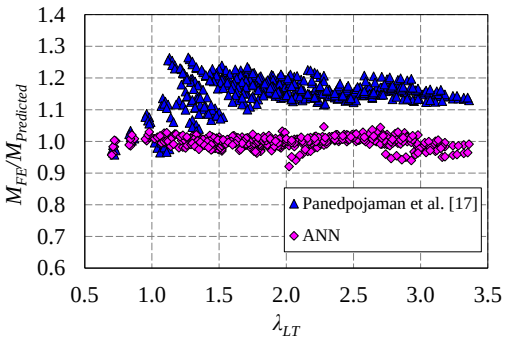

(c) ANN vs. Panedpojaman et al. [15]

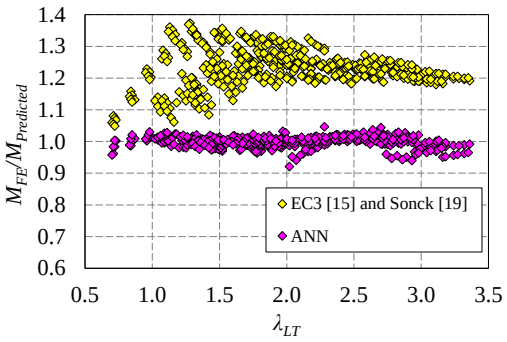

(d) ANN vs. EC3 [13] and Sonck [17]

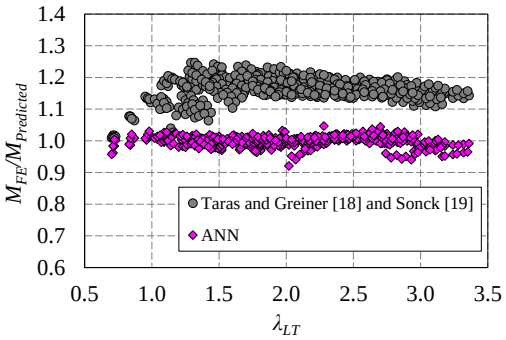

(e) ANN vs. Taras and Greiner [16] with Sonck [17]

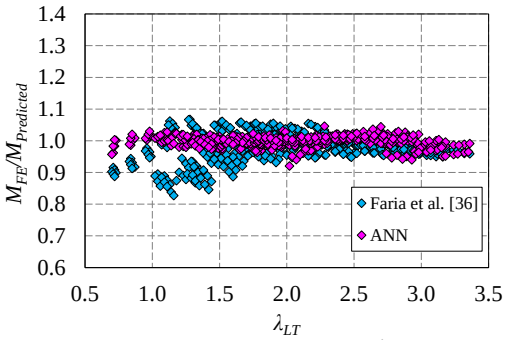

(f) ANN vs. Faria et al. [41]

Fig. 9: Loads applied at shear centre

According to **Fig. 9a**, it is possible to notice that most finite element models presented higher moment values ($M_{FE}/M_{Predicted}$>1.0) when compared to the EC3 prediction [13]. The maximum and minimum difference (M_{FE}-$M_{Predicted}$) between the models in this comparison were 10.74 kN.m and -16.32 kN.m, respectively. It is noteworthy that to calculate the moment, according to EC3 [13] requirements, for values d_g/b_f>1.2, the buckling curve *b* must be used. In this context, EC3 [13] recommendations may underestimate the LTB resistance of steel cellular beams. One way to reduce these differences is to use the buckling curve *c*, as presented in Ferreira et al. [37].

Regarding the AS 4100-1998 [14], as shown in **Fig. 9b**, for λ_{LT}≤2.0, values of the ratio $M_{FE}/M_{Predicted}$<1.0 were obtained. This was due to the drop in resistance of the cellular steel beams as a result of the combination of the LTB with some local buckling mode, such as web-post buckling or web distortional buckling. On the other hand, for λ_{LT}>2.0, the values of the ratio $M_{FE}/M_{Predicted}$ increase, situation in which the models presented LTB failure. According to Ellobody [1], the Australian standard underestimates the LTB resistance of steel cellular beams, which is in fact consistent with the analyses carried out in the present study. The maximum and minimum differences (M_{FE}-$M_{Predicted}$) between the models, in this case were 32.74 kN.m and -14.26 kN.m, respectively.

The proposal by Panedpojaman et al.[15], which is based on EC3, underestimates the LTB resistance of steel cellular beams (**Fig. 9c)**. However, this occurred for λ_{LT}>1.5, models in which ratio values were $M_{FE}/M_{Predicted}$>1.1, were verified. It is noteworthy that the authors' proposal takes into account a correction factor due to the absence (uniform bending), or the presence (mid-span and uniformly distributed loads) of the shear effect. The minimum and maximum values calculated through the difference between the numerical model and the predicted one were -20.93 kN.m and 4.38 kN.m, respectively.

The comparison of finite element models with the predictions of EC3 [13] and Sonck [17], Taras and Greiner [16] with Sonck [17] are presented in **Figs. 9d-e**, respectively. These models, developed in accord with EC3, consist of modifying the imperfection factor which is calculated in function of the ratio between the elastic section modulus in both main strong and weak axis. Both methods underestimated the LTB resistance of steel cellular beams. In the case of the EC3 [13] with Sonck [17] procedure, the $M_{FE}/M_{Predicted}$ ratio reached the value of approximately 1.4, while in the proposal by Taras and Greiner [16] with Sonck [17], this value reached 1.25, approximately. The maximum and minimum differences (M_{FE}-$M_{Predicted}$), respectively, between the models were

-4.66 kN.m and -27.16kN.m, for EC3 [13] with Sonck [17], and for Taras and Greiner [16] with Sonck [17] theses values were -0.82 kN.m and -19.78kN.m.

Fig. 9f shows the comparison between finite element models with a proposal developed by por Faria et al. [41]. This model was the one that least underestimated the LTB resistance of steel cellular beams. However, for values of $\lambda_{LT} \leq 2.0$, the predictions overestimated the resistance of steel cellular beams, especially for the models in which LTB was verified accompanied by local buckling modes. The minimum and maximum values calculated through the difference between the numerical model and the predicted one were -20.88 kN.m and -6.33 kN.m, respectively. **Table 5** presents the summary of statistical analyses. **Fig. 10** shows the relative error between the 458 models that were compared.

Table 5: Comparison of statistical values to evaluate the accuracy of the ANN models with different procedures for loads applied at shear centre

Reference	[13]	[14]	[15]	[13] and [17]	[16] and [17]	[41]	ANN
Average	1.099	1.028	1.153	1.233	1.164	0.979	0.998
S.D.	6.04%	7.57%	5.41%	5.94%	3.86%	4.51%	1.70%
Var.	0.36%	0.57%	0.29%	0.35%	0.15%	0.20%	0.03%
Max.	1.195	1.166	1.265	1.373	1.247	1.068	1.046
Min.	0.903	0.753	0.958	1.049	1.008	0.827	0.921
R^2	0.9935	0.9858	0.9922	0.9964	0.9968	0.9958	0.9998
RMSE	10.0913	16.7249	16.9338	22.6819	19.1778	14.1996	1.4816
MAE	7.6783	7.3541	12.1673	17.0621	13.6899	5.9913	0.9703

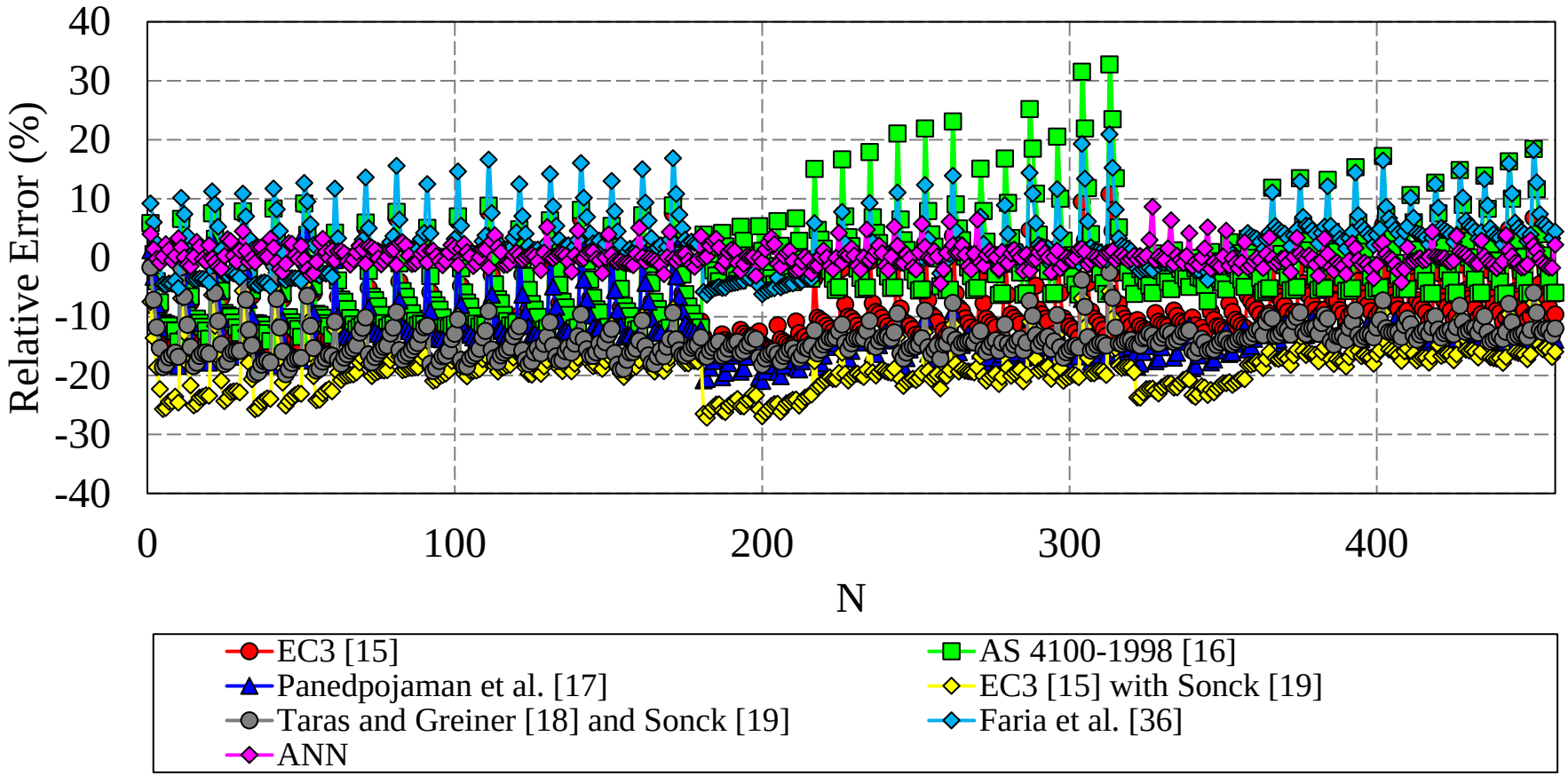

Fig. 10: Relative error (%) between the models considering loads applied at shear centre

6.2. LOADS APPLIED AT UPPER FLANGE

For loads applied at upper flange, the ANN formula is compared with EC3 [46], AS 4100-1998 [14] and Taras and Greiner [16] with Sonck [17]. In the latter case, the equation of the three factors (C_1, C_2 and C_3) is used to calculate the critical moment [46]. In this scenario, in total of 768 selected models, 310 models were subjected to loading applied at upper flange. The comparation results are shown in **Fig. 11**.

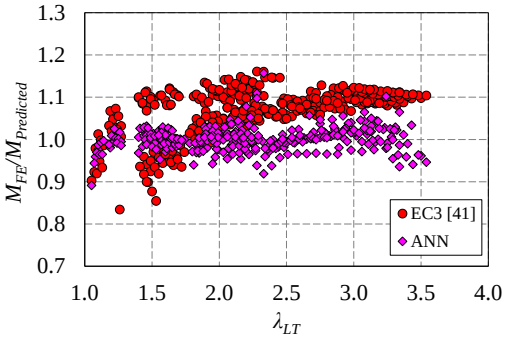

(a) ANN vs. EC3 [46]

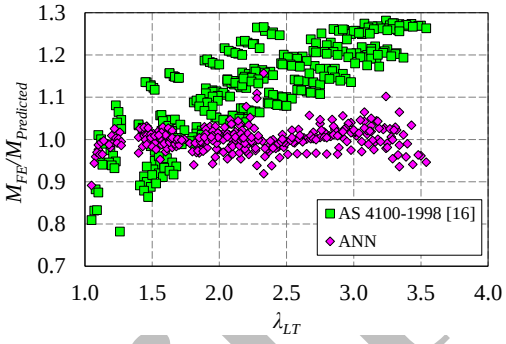

(b) ANN vs. AS 4100-1998 [14]

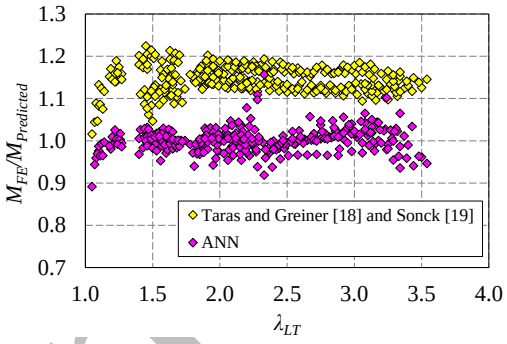

(c) ANN vs. Taras and Greiner [16] and Sonck [17]

Fig. 11: Loads applied at upper flange

When comparing the finite models with the EC3 [46] (**Fig. 11a**), for $\lambda_{LT} \leq 1.8$ the procedure overestimates the LTB resistance of steel cellular beams subjected to the destabilizing effect of loading. It is noteworthy that the smaller the value of λ_{LT}, the greater the possibility of the steel cellular beam reaching the LTB mode in the combination with the other buckling modes, such as WPB or WDB. In this context, the minimum and maximum differences between the finite element model and the predicted by EC3 were - 13.86 kN.m and 19.84 kN.m, respectively. On the other hand, when the numerical models were compared with the Australian standards [14] (**Fig. 11b**), it proved to underestimate the resistance of the cellular beams for $\lambda_{LT} > 1.5$, and the difference could reach, approximately, 30% more than the resistance of the finite element model. This procedure showed the minimum and maximum values between the numerical model and the predicted model (M_{FE}-$M_{Predicted}$) equal -21.96 kN.m and 27.83 kN.m, respectively.

Finally, when comparing finite element models with Taras and Greiner [16] with Sonck [17], considering the equation of the three factors (C_1, C_2 and C_3) [46], the analytical procedure showed results in which the ratio $M_{FE}/M_{Predicted}$ varied between 1.00 and 1.22, demonstrating that all results are in favor of safety, although in some models the LTB resistance of steel cellular beams may be underestimated. In this case, the minimum and maximum values between the numerical model and the predicted were -

18.33 kN.m and 0.22 kN.m, respectively. **Table 6** presents the summary of the statistical analyses, and **Fig. 12** illustrates the relative error between the 310 models that were compared. **Table 6** presents the summary of statistical analyses, and **Fig. 12** illustrates the relative error between the 310 models that were compared.

Table 6: Comparison of statistical values to evaluate the accuracy of the ANN models with different procedures for loads applied at upper flange

Reference	[46]	[14]	[16] with [17]	ANN
Average	1.064	1.116	1.145	1.001
S.D.	5.85%	10.75%	3.31%	2.87%
Var.	0.34%	1.16%	0.11%	0.08%
Max.	1.161	1.281	1.224	1.157
Min.	0.834	0.782	1.002	0.891
R^2	0.9921	0.982	0.9973	0.9994
RMSE	8.3819	12.1456	12.2539	1.9315
MAE	5.0446	7.9363	9.1867	1.2298

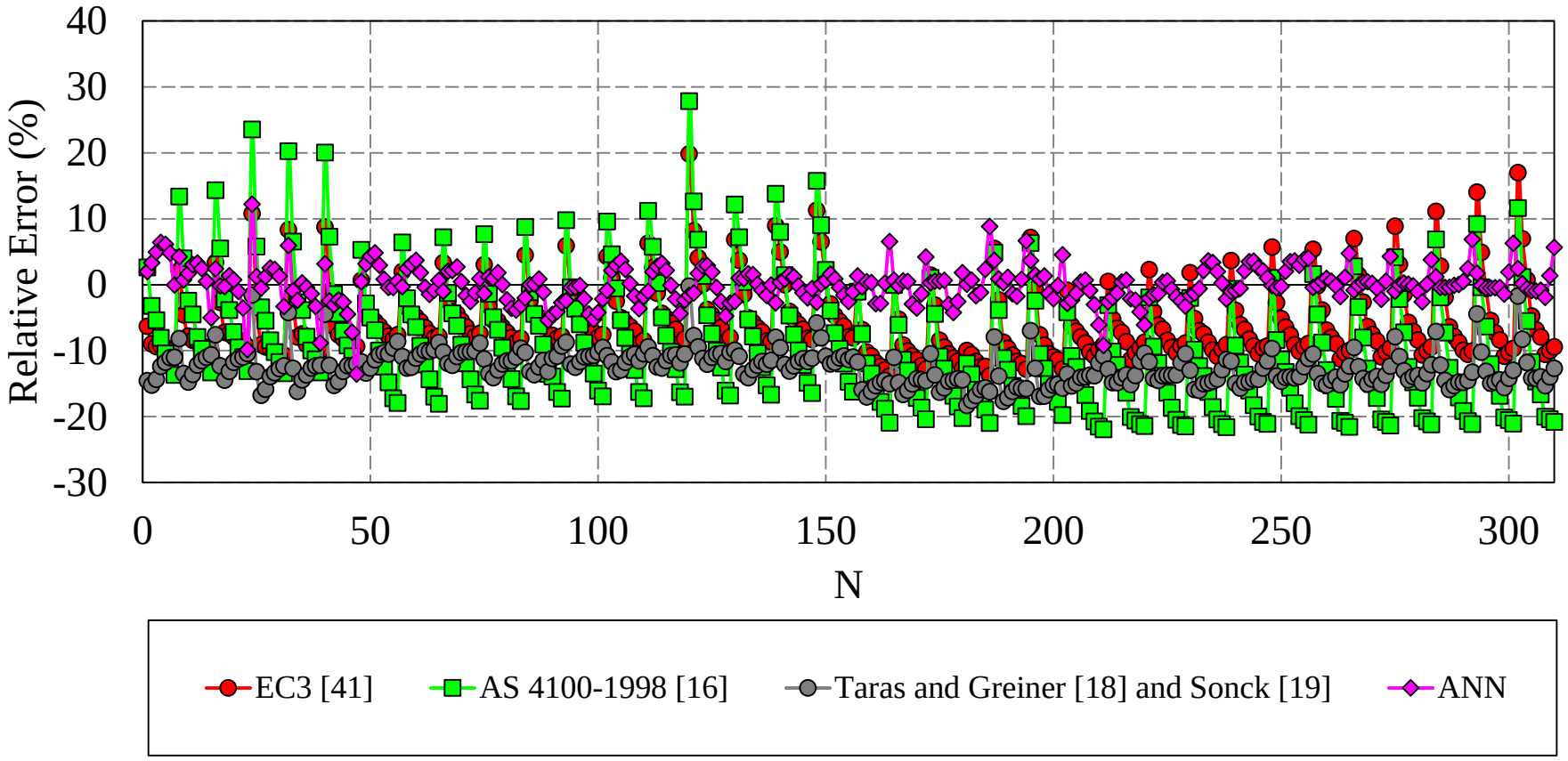

Fig. 12: Relative error (%) between the models considering loads applied at upper flange

CONCLUSION

This paper develops a robust numerical model for predicting the lateral-torsional buckling behavior of steel cellular beams, also considering the interaction of LTB mode with the web post buckling and web distortional buckling. The finite element model was calibrated via tests consolidated in the literature and a parametric study which was carried out through post-buckling analysis, considering physical and geometric imperfections as well as destabilizing loading effects. 768 models were selected to generate the ANN-based formula while the accuracy of this ANN-based model can be further improved by adding more data from future experimental and numerical studies, and makes this ANN model flexible enough to improve overtime. The proposed ANN-based model produces a single output, which is the LTB resistant moment of steel cellular beams, accounting for the length, overall height of the beam, opening diameter, distance between opening, flange width, flange thickness, web thickness, distance from the point of the load application to the shear centre of the section, and the moment-gradient factor. The finite element models were compared with the ANN-based formula and six analytical procedures, considering neutral and destabilizing effects of loads. The Australian standards underestimated the lateral-torsional buckling resistance of steel cellular beams. Regarding the analytical models based on EC3, most of them underestimated the resistance prediction of steel cellular beams. Finally, the ANN-based formula showed agreement with the finite element models. While the entire process of ANN model generation is indeed laborious and requires a level of expertise on numerical computing, its application for the design of real structures is simple. The model can be easily implemented in a spreadsheet or any other programming environment, using the provided weights and biases. Compared to the procedures provided by design guidelines and codes of practices, which often require iterative processes in order to determine the equilibrium of internal forces inside the cross section under conditions of combined axial force and bending moment, the implementation of the ANN model instead, could be straightforward while the computational cost is low.

REFERENCES

[1] Ellobody E. Nonlinear analysis of cellular steel beams under combined buckling modes. Thin-Walled Struct 2012;52:66–79. https://doi.org/10.1016/j.tws.2011.12.009.

[2] El-Sawy KM, Sweedan AMI, Martini MI. Moment gradient factor of cellular steel beams under inelastic flexure. J Constr Steel Res 2014;98:20–34. https://doi.org/10.1016/j.jcsr.2014.02.007.

[3] Ferreira FPV, Rossi A, Martins CH. Lateral-torsional buckling of cellular beams according to the possible updating of EC3. J Constr Steel Res 2019;153:222–42. https://doi.org/10.1016/j.jcsr.2018.10.011.

[4] Bradford MA. Distortional buckling of monosymmetric I-beams. J Constr Steel Res 1985;5:123–36. https://doi.org/10.1016/0143-974X(85)90010-0.

[5] Bradford MA. Inelastic distortional buckling of I-beams. Comput Struct 1986;24:923–33. https://doi.org/10.1016/0045-7949(86)90300-7.

[6] Bradford MA. Buckling of elastically restrained beams with web distortions. Thin-Walled Struct 1988;6:287–304. https://doi.org/10.1016/0263-8231(88)90005-5.

[7] Bradford MA. Buckling of doubly-symmetric cantilevers with slender webs. Eng Struct 1992;14:327–34. https://doi.org/10.1016/0141-0296(92)90046-S.

[8] Kerdal D, Nethercot DA. Failure modes for castellated beams. J Constr Steel Res 1984;4:295–315.

https://doi.org/10.1016/0143-974X(84)90004-X.

[9] Tsavdaridis KD, D'Mello C. Web buckling study of the behaviour and strength of perforated steel beams with different novel web opening shapes. J Constr Steel Res 2011;67:1605–20. https://doi.org/10.1016/j.jcsr.2011.04.004.

[10] Erdal F, Saka MP. Ultimate load carrying capacity of optimally designed steel cellular beams. J Constr Steel Res 2013;80:355–68. https://doi.org/10.1016/j.jcsr.2012.10.007.

[11] Panedpojaman P, Thepchatri T, Limkatanyu S. Novel design equations for shear strength of local web-post buckling in cellular beams. Thin-Walled Struct 2014;76:92–104. https://doi.org/10.1016/j.tws.2013.11.007.

[12] Grilo LF, Fakury RH, Castro e Silva ALR de, Veríssimo G de S. Design procedure for the web-post buckling of steel cellular beams. J Constr Steel Res 2018;148:525–41. https://doi.org/10.1016/j.jcsr.2018.06.020.

[13] European committee for standardization. EUROCODE 3: Design of steel structures - Part 1-1: General rules and rules buildings 2005.

[14] Standards Association of Australia. AS 4100-1998 Steel Structures 2016.

[15] Panedpojaman P, Sae-Long W, Chub-Uppakarn T. Cellular beam design for resistance to inelastic lateral-torsional buckling. Thin-Walled Struct 2016;99:182–94. https://doi.org/10.1016/j.tws.2015.08.026.

[16] Taras A, Greiner R. New design curves for lateral-torsional buckling-Proposal based on a consistent derivation. J Constr Steel Res 2010;66:648–63. https://doi.org/10.1016/j.jcsr.2010.01.011.

[17] Sonck D. Global buckling of castelled and cellular steel beams and columns. 2014. Ph.D. thesis. Ghent University, 2014.

[18] Özcan F, Atiş CD, Karahan O, Uncuoğlu E, Tanyildizi H. Comparison of artificial neural network and fuzzy logic models for prediction of long-term compressive strength of silica fume concrete. Adv Eng Softw 2009;40:856–63. https://doi.org/10.1016/j.advengsoft.2009.01.005.

[19] Golafshani EM, Rahai A, Sebt MH, Akbarpour H. Prediction of bond strength of spliced steel bars in concrete using artificial neural network and fuzzy logic. Constr Build Mater 2012;36:411–8. https://doi.org/10.1016/j.conbuildmat.2012.04.046.

[20] Limbachiya V, Shamass R. Application of Artificial Neural Networks for web-post shear resistance of cellular steel beams. Thin-Walled Struct 2021;161:107414. https://doi.org/10.1016/j.tws.2020.107414.

[21] Lawson RM, Hicks SJ. Design of composite beams with large web openings. SCI P355. The Steel Construction Institute; 2011.

[22] Nguyen T-A, Ly H-B, Tran VQ. Investigation of ANN Architecture for Predicting Load-Carrying Capacity of Castellated Steel Beams. Complexity 2021;2021:1–14. https://doi.org/10.1155/2021/6697923.

[23] Hosseinpour M, Sharifi Y, Sharifi H. Neural network application for distortional buckling capacity assessment of castellated steel beams. Structures 2020;27:1174–83. https://doi.org/10.1016/j.istruc.2020.07.027.

[24] Sharifi Y, Moghbeli A, Hosseinpour M, Sharifi H. Study of Neural Network Models for the Ultimate Capacities of Cellular Steel Beams. Iran J Sci Technol Trans Civ Eng 2020;44:579–89. https://doi.org/10.1007/s40996-019-00281-z.

[25] Abambres M, Rajana K, Tsavdaridis K, Ribeiro T. Neural Network-Based Formula for the Buckling Load Prediction of I-Section Cellular Steel Beams. Computers 2018;8:2. https://doi.org/10.3390/computers8010002.

[26] Sharifi Y, Moghbeli A, Hosseinpour M, Sharifi H. Neural networks for lateral torsional buckling strength assessment of cellular steel I-beams. Adv Struct Eng 2019;22:2192–202. https://doi.org/10.1177/1369433219836176.

[27] Tohidi S, Sharifi Y. Inelastic lateral-torsional buckling capacity of corroded web opening steel beams using artificial neural networks. IES J Part A Civ Struct Eng 2015;8:24–40. https://doi.org/10.1080/19373260.2014.955139.

[28] Gholizadeh S, Pirmoz A, Attarnejad R. Assessment of load carrying capacity of castellated steel beams by neural networks. J Constr Steel Res 2011;67:770–9. https://doi.org/10.1016/j.jcsr.2011.01.001.

[29] Tohidi S, Sharifi Y. Neural networks for inelastic distortional buckling capacity assessment of steel I-beams. Thin-Walled Struct 2015;94:359–71. https://doi.org/10.1016/j.tws.2015.04.023.

[30] American Institute of Steel Construction. ANSI/AISC 360-16 - Specification for structural steel buildings. 2016.

[31] Sonck D, Belis J. Lateral-torsional buckling resistance of cellular beams. J Constr Steel Res 2015;105:119–28. https://doi.org/10.1016/j.jcsr.2014.11.003.

[32] Boissonnade N, Nseir J, Lo M, Somja H. Design of cellular beams against lateral torsional buckling. Proc Inst Civ Eng - Struct Build 2013;167:436–44. https://doi.org/10.1680/stbu.12.00049.

[33] Nseir J, Lo M, Sonck D, Somja H, Vassart O, Boissonnade N. Lateral Torsional Buckling of Cellular Steel Beams. Annu. Stab. Conf. Struct. Stab. Res. Counc., Grapevine, Texas: 2012.

[34] Sweedan AMI. Elastic lateral stability of I-shaped cellular steel beams. J Constr Steel Res 2011;67:151–63. https://doi.org/10.1016/j.jcsr.2010.08.009.

[35] Sonck D, Vanlaere W, Van Impe R. Influence of plasticity on lateral–torsional buckling behaviour of cellular beams. Mater Res Innov 2011;15:s158–61. https://doi.org/10.1179/143307511X12858956847958.

[36] Rajana K, Tsavdaridis KD, Koltsakis E. Elastic and inelastic buckling of steel cellular beams under strong-axis bending. Thin-Walled Struct 2020;156:106955. https://doi.org/10.1016/j.tws.2020.106955.

[37] Ferreira FPV, Martins CH. LRFD for Lateral-Torsional Buckling Resistance of Cellular Beams. Int J Civ Eng 2020;18:303–23. https://doi.org/10.1007/s40999-019-00474-7.

[38] Bhat RA, Gupta LM. Moment-Gradient Factor for Perforated Cellular Steel Beams Under Lateral Torsional Buckling. Arab J Sci Eng 2020;45:8727–43. https://doi.org/10.1007/s13369-020-04836-5.

[39] Khatri AP, Katikala SR, Kotapati VK. Effect of load height on elastic buckling behavior of I-shaped cellular beams. Structures 2021;33:1923–35. https://doi.org/10.1016/j.istruc.2021.05.047.

[40] Bhat RA, Gupta LM. Interaction of Buckling Modes for Cellular Steel Beams Under Flexure. Int J Steel Struct 2021;21:260–73. https://doi.org/10.1007/s13296-020-00437-y.

[41] Correa de Faria C, Carvalho H, Hallal Fakury R, Figueiredo Grilo L. Lateral-torsional buckling resistance of cellular steel beams at room temperature and fire situation. Eng Struct 2021;237:112046. https://doi.org/10.1016/j.engstruct.2021.112046.

[42] Kirby P, Nethercot D. Design for structural stability. Suffolk: Granada Publishing; 1979.

[43] Timoshenko S, Gere J, Timoshenko S. Theory of elastic stability. 2nd ed. New York, N. Y.: McGraw-Hill Book Company; 1961.

[44] ACB+. ArcelorMittal Cellular Beams Software ACB+ v2 02. Long Carbon Eur Res Centre, Arcelor Mittal 2010.

[45] European committee for standardization. EN 1993-1-5: Eurocode 3 – Design of steel structures – Part 1-5: Plated structural elements. 2006.

[46] European committee for standardization. EN 1993-1-1: Eurocode 3 – Design of steel structures – Part 1-1: General rules and rules for buildings 2002.

[47] IS800. Indian Standard Code of Practice for General Construction in Steel 2007.

[48] Surtees JO, Liu Z. Loading Tests on Cellform Beams : Research Report. Univ Leeds 1995.

[49] Warren JJ. Ultimate load and deflection behaviour of cellular beams. 2001. M.Sc. thesis. University of Natal, 2001.

[50] Dassault Systèmes Simulia. Abaqus 6.18 2016.

[51] Ferreira FPV, Tsavdaridis KD, Martins CH, De Nardin S. Buckling and post-buckling analyses of composite cellular beams. Compos Struct 2021;262. https://doi.org/10.1016/j.compstruct.2021.113616.

[52] Sonck D, Van Impe R, Belis J. Experimental investigation of residual stresses in steel cellular and castellated members. Constr Build Mater 2014;54:512–9. https://doi.org/10.1016/j.conbuildmat.2013.12.045.

[53] Ferreira FPV, Martins CH, De Nardin S. Assessment of web post buckling resistance in steel-concrete composite cellular beams. Thin-Walled Struct 2021;158:106969. https://doi.org/10.1016/j.tws.2020.106969.

[54] Ahmad A, Cotsovos DM, Lagaros ND. Assessing the reliability of RC code predictions through the use of artificial neural network. 1st Int. Conf. Struct. Saf. under fire blast, Glasgow, UK: 2016.

[55] MATLAB and Statistics Toolbox Release 2019a. The MathWorks, Inc., Natick, Massachusetts, United States 2019.

[56] Jin J, Li M, Jin L. Data Normalization to Accelerate Training for Linear Neural Net to Predict Tropical Cyclone Tracks. Math Probl Eng 2015;2015:1–8. https://doi.org/10.1155/2015/931629.

[57] Moradi MJ, Khaleghi M, Salimi J, Farhangi V, Ramezanianpour AM. Predicting the compressive strength of concrete containing metakaolin with different properties using ANN. Measurement 2021;183:109790. https://doi.org/10.1016/j.measurement.2021.109790.

[58] Olden JD, Jackson DA. Illuminating the "black box": a randomization approach for understanding variable contributions in artificial neural networks. Ecol Modell 2002;154:135–50. https://doi.org/10.1016/S0304-3800(02)00064-9.

[59] Olden JD, Joy MK, Death RG. An accurate comparison of methods for quantifying variable importance in artificial neural networks using simulated data. Ecol Modell 2004;178:389–97. https://doi.org/10.1016/j.ecolmodel.2004.03.013.

[60] Garson DG. Interpreting neural network connection weights. 1991.

[61] Gupta T, Patel KA, Siddique S, Sharma RK, Chaudhary S. Prediction of mechanical properties of rubberised concrete exposed to elevated temperature using ANN. Measurement 2019;147:106870. https://doi.org/10.1016/j.measurement.2019.106870.

[62] Sharifi Y, Moghbeli A. Shear capacity assessment of steel fiber reinforced concrete beams using artificial neural network. Innov Infrastruct Solut 2021;6:89. https://doi.org/10.1007/s41062-021-00457-5.

[63] al-Swaidani AM, Khwies WT. Applicability of Artificial Neural Networks to Predict Mechanical and Permeability Properties of Volcanic Scoria-Based Concrete. Adv Civ Eng 2018;2018:1–16. https://doi.org/10.1155/2018/5207962.